Phonon-mediated decay of metal surface states

A. Eiguren,[1] B. Hellsing,[2,3] E. V. Chulkov,[1,3] and P. M. Echenique[1,3]
[1]*Departmento de Física de Materiales and Centro Mixto CSIC-UPV/EHU, Facultad de Ciencias Químicas, Universidad del Pais Vasco/Euskal Herriko Unibertsitatea, Adpo. 1072, 20018 San Sebastián/Donostia, Basque Country, Spain*
[2]*Department of Physics, Chalmers University of Technology and Göteborg University, S-412 96 Göteborg, Sweden*
[3]*Donostia International Physics Center (DIPC), Paseo de Manuel Lardizabal, 4, 20018 San Sebastián/Donostia, Spain*
(Received 30 January 2003; published 27 June 2003)

We present results of a theoretical investigation of the phonon-mediated decay of metal surface states. The calculated energy- and temperature-dependent lifetime broadening of a hole as well as the electron-phonon coupling parameter for the surface-state band on Al(100), Ag(111), Cu(111) and Au(111) are given. A detailed analysis of the Eliashberg spectral function shows that the intraband scattering is of minor importance for these systems. The surface Rayleigh phonon mode is shown to be crucial for the surface-state decay on the noble metal surfaces, in particular for energies close to the Fermi level where the Rayleigh mode is responsible for the major part of the phonon induced lifetime broadening.

DOI: 10.1103/PhysRevB.67.235423 PACS number(s): 73.20.−r, 63.20.Kr, 72.15.Lh, 73.25.+i

I. INTRODUCTION

During the last few years many experimental and theoretical work have been focused on dynamical processes at metal surfaces (see, for instance, Refs. 1–11). The present investigation of the phonon-mediated decay of electronic surface states is also framed in this context. Surface states are formed on single-crystal surfaces due to the presence of a band gap. The surface-state electron is trapped between the crystal potential barrier and the vacuum potential (image potential), being mostly linked to the crystal potential in contrast to the image potential.[12,13] Detailed investigations of the inherent interactions, electron-electron (e-e) and electron-phonon (e-p), responsible for the finite lifetime of excited electrons (holes) in surface states, are crucial for the understanding of quasiparticle dynamics on metal surfaces. Recent measurements performed by scanning tunneling microscopy (STM),[3,14–20] high resolution angular-resolved photoemission spectroscopy (PES) experiments,[21–28] and time-resolved two-photon photoemission spectroscopy (TR-2PPE) (Refs. 29 and 30) allow a detailed comparison with theoretical calculations.[14,26,31] In this paper we study the decay of a surface hole state due to the e-p scattering, taking into account in principle all the phonon modes and electron wave functions of the system. The surface-localized nature of the surface state itself and some phonon modes give rise to a particular mixture of dimensionalities in the character of the interaction. A surface hole state might decay via intraband transition to the surface state itself [two-dimensional (2D) character] or into bulk states (3D character).

In Sec. II we apply the Fröhlich perturbation treatment to the surface-state decay problem and present some general arguments to show why the conventional Bloch perturbation treatment fails. The choice of unperturbed electron and phonon systems and the approximations included in the calculations will be presented in Sec. III. Finally, in Sec. IV we first investigate the role of electronic screening, comparing the results obtained when considering simple Thomas-Fermi and random-phase-approximation (RPA) dielectric response. In addition, we point out the nonphysical divergence appearing for intraband scattering when considering the Bloch perturbation picture and show that a proper strategy is to make use of the Fröhlich description. This section is closed by giving results from a detailed analysis of the electron-phonon (e-p) coupling contribution to the lifetime broadening and the e-p coupling parameter λ for surface hole states of Al(100), Ag(111), and Cu(111).

II. THEORY

The many-body theory of the electron-phonon interaction developed during last 50 years is well documented in a number of books and reviews (see, for instance, Refs. 32–35) and describes this interaction mostly in bulk materials. In this section we present a comprehensive formulation based on the perturbation theory focusing mostly in the fundamental differences between surface and bulk. Later on this theory will be used in the e-p coupling calculations.

As usual in any perturbation theory, it is necessary to define the ''manageable'' unperturbed part of the interacting systems, and then the interaction as a ''small'' perturbation between, in our case, the electrons and phonons. Different choices of unperturbed Hamiltonians obviously lead to different descriptions. Within the Born-Oppenheimer approximation (Adiabatic approximation),[34] the electron and phonon systems are separated, as the valence electrons are assumed to adjust instantaneously to the ionic positions. In order to take into account the nonadiabatic effects related to the e-p coupling, the full electron Hamiltonian is written as the sum of an unperturbed Hamiltonian plus a perturbation. In general, this Hamiltonian depends on the instantaneous ionic positions $[\vec{R}_\alpha]$,

$$H_e(\vec{r},[\vec{R}_\alpha]) = H_e^0(\vec{r},[\vec{R}_\alpha]) + H_{e-p}(\vec{r},[\vec{R}_\alpha]). \qquad (1)$$

Different descriptions relate to different ways to decompose the right-hand side of Eq. (1). It is clear that the most adequate definition of H_e and H_e^0 is the one that takes better

 ©2003 The American Physical Society

into account the nearly adiabatic motion of electrons following the slow ionic motion. This point will be of crucial importance for the understanding of the decay of the surface hole state via transitions within the surface band itself *(intraband scattering)*.

However, the most common procedure is to choose the unperturbed electron Hamiltonian (H_e^0) as the one corresponding to the rigid lattice in its equilibrium structure. This procedure is known in the literature as the Bloch description of the electron-phonon interaction.[34] The treatment introduced by Fröhlich and applied in this work considers the unperturbed electron system ''moving'' adiabatically with the ions.[34] The applicability of this procedure is justified in Sec. IV.

A. Perturbation treatment

The ideas on which the Fröhlich description is based on are quite old. For example it has been used in the work by Mitra[36] where the electron-phonon matrix element was analyzed in the context of the tight-binding approximation.

The total electronic Hamiltonian, Eq. (1), can be written as

$$H_e(\vec{r},\vec{R}_\alpha)=-\frac{\nabla^2}{2}+\sum_\alpha v_s(\vec{r}-\vec{R}_\alpha)$$

$$=-\frac{\nabla^2}{2}+\sum_\alpha e^{-\vec{u}_\alpha\cdot\vec{\nabla}_R}\cdot v_s(\vec{r}-\vec{R}_\alpha^0), \qquad (2)$$

where

$$\vec{u}_\alpha=\vec{R}_\alpha-\vec{R}_\alpha^0, \qquad (3)$$

v_s is the screened pseudopotential,

$$v_s(\vec{r})=\int d\vec{r}\,'\,\epsilon^{-1}(\vec{r},\vec{r}\,')\cdot v(\vec{r}\,'), \qquad (4)$$

$v(\vec{r})$ is the bare pseudo potential, and $\epsilon^{-1}(\vec{r},\vec{r}\,')$ is the inverse of the static dielectric function. In general, electron self-consistent Hamiltonians can be represented in the form of Eq. (1) only for periodic systems. For systems with atoms moved from its equilibrium positions this decomposition is not valid. However, such a decomposition is still conserved for metals with atoms out of the equilibrium positions if the interaction between sp electrons and ions is supposed to be weak.[37] In the present work we describe this interaction by using a local Ashcrof pseupodotential[38] screened by Thomas-Fermi and RPA dielectric function in the calculations of the deformation potentials (gradient of the screened potential).

The exponential factor in Eq. (2) translates the screened pseudopotential through the vector $\vec{u}_\alpha$ from the equilibrium position $\vec{R}_\alpha^0$ to the instantaneous position $\vec{R}_\alpha$ and corresponds to an infinite order Taylor expansion around the equilibrium ionic positions. Splitting Eq. (2) according to the Fröhlich description we have that the unperturbed electronic Hamiltonian is

$$H_{e,F}^0(\vec{r},[\vec{R}_\alpha])=-\frac{\nabla^2}{2}+\sum_\alpha e^{-\vec{U}\cdot\vec{\nabla}_R}v_s(\vec{r}-\vec{R}_\alpha^0), \qquad (5)$$

and the perturbation is the difference between Eq. (2) and Eq. (5):

$$H_{e-p,F}(\vec{r},\vec{R}_\alpha)\equiv H_e^0-H_{e,F}^0$$

$$=\sum_\alpha [e^{-\vec{u}_\alpha\cdot\vec{\nabla}_R}-e^{-\vec{U}\cdot\vec{\nabla}_R}]v_s(\vec{r}-\vec{R}_\alpha^0)$$

$$=\sum_\alpha [e^{-(\vec{u}_\alpha-\vec{U})\cdot\vec{\nabla}_R}-1]v_s[\vec{r}-(\vec{R}_\alpha^0+\vec{U})]. \qquad (6)$$

Note in Eq. (5) that the one-electron potential is displaced through the vector $\vec{U}$ with respect to the Bloch description [$\vec{U}=0$, Eq. (39)]. As the surface state is localized within a few layers close to the surface, we define $\vec{U}$ as the mean displacement of these layers. We define

$$\vec{U}\equiv\sum_{\beta=1}^{\tilde{N}_z}\vec{u}_\beta/\tilde{N}_z, \qquad (7)$$

where $\tilde{N}_z$ is the number of layers (surface and below) where the surface-state wave function has an appreciable amplitude. For a ''high-energy'' phonon mode propagating perpendicular to the surface, this mean value becomes negligible due to the rapid oscillations of the polarization vectors from layer to layer, but approaching the $\vec{q}\to 0$ and $\omega\to 0$ limit, the motions of ions are almost in phase and $\vec{U}$ is no longer negligible.

In the Bloch description ($\vec{U}=0$) the unperturbed Hamiltonian and electron wave functions refer to the rigid lattice and are independent of the considered phonon mode. In the Fröhlich description the effect of the rigid translations of the crystal is contained in the unperturbed Hamiltonian and thus takes into account that a rigid motion of the lattice (in the $\vec{q}\to 0$ and $\omega\to 0$ limit) does not involve a perturbation of the electronic system.

In the work by S. Andersson and co-workers,[39,40] this fact is taken into account in a simple and original way. The authors considered the problem of the long-range e-p interaction applying a simple one-dimensional model where only relative motions of the surface layers are taken into account. In this way, they avoided the phonon modes associated with rigid translations of the crystal.

In the case of a surface hole state scattering to a bulk band state (*interband scattering*), this limit is never reached and both descriptions, Bloch's and Fröhlich's, give similar results. From the results presented in Sec. IV, it is clear that the intraband scattering is of minor importance compared with interband scattering. As we have argued in previous works,[31,41] a reasonable approximation for a surface hole state with a small momentum $k_i<10^{-1}$ (a.u.)] is to treat the interband scattering in the Bloch description and neglect the intraband contribution. However, in this work we will show this explicitly by treating the intraband scattering properly applying the Fröhlich perturbation picture.

B. Lifetime broadening and λ parameter

In this section we give some equations which form the basis for the calculations in subsequent sections (Appendix A contains more details). We will express the information related to *e-p* interaction in terms of the spectral Eliashberg functions defined for phonon emission and absorption processes. The Eliashberg function is proportional to the probability to transfer an energy ω at $T=0$. The Eliashberg functions corresponding to emission (E) and absorption (A) of phonons are written as

$$\alpha^2F^E_{i,\vec{k}_i}(\omega)=\int d^2\vec{q}\sum_{f,\nu}|g^{i,f}_{\vec{q},\nu}|^2\delta(\epsilon_{i,\vec{k}_i}-\epsilon_{f,\vec{k}_i-\vec{q}}-\omega_{\vec{q},\nu})\times\delta(\omega-\omega_{\vec{q},\nu}), \tag{8}$$

$$\alpha^2F^A_{i,\vec{k}_i}(\omega)=\int d^2\vec{q}\sum_{f,\nu}|g^{i,f}_{\vec{q},\nu}|^2\delta(\epsilon_{i,\vec{k}_i}-\epsilon_{f,\vec{k}_i-\vec{q}}+\omega_{\vec{q},\nu})\times\delta(\omega-\omega_{\vec{q},\nu}). \tag{9}$$

The *e-p* coupling function in Eqs. (8) and (9) (from Appendix A) is given by the matrix element

$$g^{i,f}_{\vec{q},\nu}\equiv\sqrt{\frac{1}{2M\omega_{\vec{q},\nu}\Omega_0}}\int dz\,\phi_i(z)G_{\vec{q}}(z)\phi_f(z), \tag{10}$$

where

$$G_{\vec{q}}(z)=\sum_{R_{\alpha,z}}\vec{\sigma}_{\vec{q},\nu}(R_{\alpha,z})\cdot e^{i\vec{q}\cdot\vec{c}}\cdot F_{2D}[\vec{\nabla}v_s(\vec{r}-\vec{R}_\alpha)], \tag{11}$$

where F_{2D} symbolizes the 2D Fourier transformation, the index i and f refer to the initial hole state (surface state) and final hole state, respectively. $\omega_{\vec{q},\nu}$ and $\vec{\sigma}_{\vec{q},\nu}$ are the phonon energy and polarization vector, respectively, Ω_0 is the area corresponding to each atomic position, and $\vec{c}$ the vector that translates one layer to the same parallel configuration as the upper (lower) layer. The phonon mode involved in the scattering event and denoted by ν has parallel momentum $\vec{q}$. The first Dirac delta function in Eqs. (8) and (9) ensures energy conservation in the scattering and the second one in these equations registers all the scattering events with energy transfer ω, summed over all possible phonon modes ν with momentum $\vec{q}$. The hole decay rate—lifetime broadening Γ—is the integral over all scattering events that conserve energy and momentum. The electron (f) and phonon (n_B) occupation numbers introduce the temperature dependence. A derivation of the expression for Γ based on the *e-p* self-energy is given in Refs. 41 and 42 and in Appendix A we present another derivation, which yields the same result, based on a Master type of equation for the electron state occupancy.[34] The result is

$$\Gamma(\epsilon_{i,\vec{k}_i})=2\pi\int_0^\infty\alpha^2F^E_{i,\vec{k}_i}(\omega)O_+(\omega,\epsilon_{i,\vec{k}_i}-\omega)+\alpha^2F^A_{i,\vec{k}_i}(\omega)O_-(\omega,\epsilon_{i,\vec{k}_i}+\omega) \tag{12}$$

with

$$O_+(\omega,\epsilon)\equiv n_B(\omega)+1-f(\epsilon), \tag{13}$$

$$O_-(\omega,\epsilon)\equiv n_B(\omega)+f(\epsilon).$$

In the literature, considering the *e-p* coupling, the interest is usually focused on superconductivity of bulk materials. In this case Eq. (12) is averaged over all initial states on the Fermi surface. In contrast, in this work we are concerned with the scattering of a specific surface hole state with a given initial energy and momentum.

A signature of the electron-phonon interaction is the linear temperature dependence at high temperatures, which is a consequence of the T dependence of the phonon occupation numbers,

$$n_B(\omega)\to\frac{k_BT}{\omega},\quad (T\to\infty). \tag{14}$$

In this limit, Eq. (12) can be written

$$\Gamma(\epsilon_{i,\vec{k}_i})=2\pi\lambda(\epsilon_{i,\vec{k}_i})k_BT, \tag{15}$$

where, according to Eq. (12) the so-called *e-p* coupling λ parameter is given by

$$\lambda(\epsilon_{i,\vec{k}_i})=\int_0^{\omega_{max}}\frac{\alpha^2F^E_{i,\vec{k}_i}(\omega)+\alpha^2F^A_{i,\vec{k}_i}(\omega)}{\omega}d\omega. \tag{16}$$

As previously pointed out, the Eliashberg function is closely related to the scattering probability transferring a given energy ω. We also resolved this probability with respect to the modulus of the momentum transfer Q. We thus define a spectral function revealing which parts of the phase space (ω, Q) contribute mostly to the scattering of a given state,

$$\alpha^2\tilde{F}_{i,\vec{k}_i}(\omega,Q)=\int d^2\vec{q}\sum_{f,\nu}|g^{i,f}_{\vec{q},\lambda}|^2\delta(\epsilon_{i,\vec{k}_i}-\epsilon_{f,\vec{k}_i-\vec{q}})\times\delta(\omega-\omega_{\vec{q},\nu})\,\delta(|\vec{q}|-Q). \tag{17}$$

In Sec. IV we analyze our calculations in terms of this function for the case of surface hole decay in Al(100) and Cu(111).

III. CALCULATION DETAILS

In this section we describe the unperturbed electron and phonon states chosen for the calculations of the *e-p* matrix elements which determine the Eliashberg function.

A. Electron states

We define the unperturbed electron system as the solutions of the one-particle Schrödinger equation applying a model potential proposed by Chulkov and co-workers[6,43,44] (see Fig. 1). This model potential $V(z)$, is constant in the plane parallel to the surface and varies only in the direction perpendicular. The potential is tuned to reproduce at the $\bar{\Gamma}$

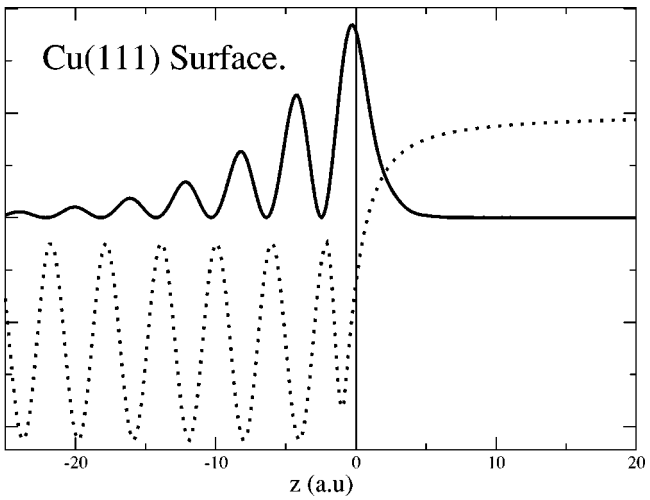

FIG. 1. Squared surface-state wave function (solid line) and the model potential (dotted line) for the Cu(111) surface.

point the correct surface projected band gap as well as the surface and first image state energies for the systems studied.

The unperturbed wave functions and energies are written

$$\psi_{n,\vec{k}}(\vec{x},z)=\phi_n(z)e^{i\vec{k}\cdot\vec{x}} \tag{18}$$

and

$$\epsilon_{k,n}=\epsilon_n+\frac{k^2}{2m}, \tag{19}$$

where

$$\frac{-1}{2}\frac{d^2}{dz^2}\phi_n(z)+V(z)\phi_n(z)=\epsilon_n^0\phi_n(z). \tag{20}$$

In Eq. (19) the electron coordinate $\vec{r}$ is separated into parallel and perpendicular components with respect to the surface $(\vec{x},z)$, and $\vec{k}$ and m are the parallel momentum and mass of the electron. In order to take into account partially the surface corrugation effect we use a realistic effective mass m^* in Eq. (19). The electron unperturbed Hamiltonian of Eq. (20) corresponds to the Bloch description of the electron-phonon interaction. To consider the Fröhlich description, the unperturbed wave functions follow the moving ions, and one must replace $\psi^0(\vec{r})$ by $\psi^0(\vec{r}-\vec{U})$ for each ionic motion pattern when calculating the e-p matrix elements.

B. Phonon states

The unperturbed phonon modes are obtained from a single force constant model, where the force constant is fitted to reproduce the elastic constants and the maximum bulk phonon frequency. This simple model leads to a dispersion relation in reasonable agreement with what is obtained from He scattering (HAS) experiments on noble metal (111) surfaces.[45] The equation of motion of an ion in position $\vec{R}$ is

$$-\omega^2\vec{u}(\vec{R}_\alpha)=\sum_\beta D_{\alpha,\beta}\vec{u}(\vec{R}_\beta), \tag{21}$$

where the so-called force-constant matrix $D_{\alpha,\beta}$ relates the force acting on the ion in position $\vec{R}_\alpha$ when an ion in the position $\vec{R}_\beta$ moves in a given direction. In a slab geometry we have solutions of the form $\vec{u}(\vec{R}_\alpha)=\vec{u}(R_{z,\alpha},\vec{q})e^{i\vec{q}\cdot\vec{R}_\alpha}$, where $\vec{q}$ is the phonon parallel momentum. An eigenvalue problem is thus obtained for the Fourier coefficients $\vec{u}(R_{z,\alpha},\vec{q})$,

$$-\omega^2\vec{u}(\vec{R}_{z,\alpha},\vec{q})=\sum_\beta \overline{D}_{\alpha,\beta}(\vec{q})\vec{u}(\vec{R}_{z,\beta},\vec{q}), \tag{22}$$

where

$$\overline{D}_{\alpha,\beta}(\vec{q})\equiv\sum_{\alpha,\beta} e^{-i\vec{q}\cdot\vec{R}_\alpha}D_{\alpha,\beta}e^{i\vec{q}\cdot\vec{R}_\beta}. \tag{23}$$

If one solves for the dynamical matrix $\overline{D}$ in a slab geometry as in the work by Black *et al.*[46] two surfaces are present. The drawback of this procedure is that the description of the phonon modes with a small momentum $q<(2\pi)/L\equiv q_c$, where L is the slab thickness, are not properly described. In the calculation of the intraband scattering contribution, this small momentum limit is always reached. To get an idea of typical values of q_c we have for Cu(111) and $N_z=30$ that $q_c\approx 0.05$ (a.u.).

A method suitable to meet the small q problem has been proposed by Trullinger.[47] The method is based on an expansion of the phonon states in terms of Gottlieb polynomials. These polynomials have the property of decaying into the bulk, thus allowing an improved representation of the surface for small momentum. The definition of the Gottlieb polynomials is[47,48]

$$\chi_n(m,\gamma)\equiv e^{-\gamma(n+m)/2}\sum_{p=0}^{n}(1-e^{\gamma})^p\binom{n}{p}\binom{m}{p} \tag{24}$$

and they satisfy the orthogonality relation

$$\sum_{m=0}^{\infty}\chi_p(m,\gamma)\chi_q(m,\gamma)=\delta_{p,q}. \tag{25}$$

The γ parameter controls the spatial decay of the polynomials into the bulk. In the Gottlieb polynomial representation the dynamical matrix and the eigenvalue problem are written

$$T(m,n,\vec{q},\gamma)\equiv\sum_{\alpha,\beta=1}^{\tilde{N}}\chi_m(\alpha,\gamma)\overline{D}_{\alpha,\beta}(\vec{q})\chi_n(\beta,\gamma) \tag{26}$$

$$-\omega^2\vec{w}_m(\vec{q})=\sum_n T(m,n,\vec{q},\gamma)\vec{w}_n(\vec{q}), \tag{27}$$

where $\tilde{N}$ is the size of the matrix. In practice, one must find a proper setting of the parameters γ and $\tilde{N}$.[48] The larger the $\tilde{N}$ value, the larger γ can be chosen corresponding to a slower decay into the bulk.[48]

Independently of the method used to calculate surface phonon modes (slab or Gottlieb polynomial method for instance), solving the corresponding eigenvalue problem, we

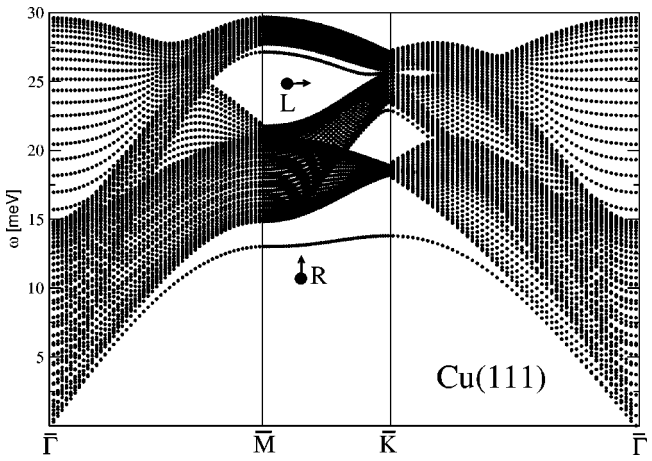

FIG. 2. Phonon dispersion of the Cu(111) surface, presented in the principal directions of the surface Brillouin zone. The polarization of the surface Rayleigh mode (**R**) and a longitudinal surface mode (**L**) are indicated by arrows. The phonon dispersion of Ag(111) is qualitatively similar.

obtain the polarization vectors $\vec{\epsilon}_{\vec{q},\nu}(R_z)$ which are complex in general and thus the ionic motion must follow an elliptic orbit,

$$\vec{u} \sim \mathrm{Re}[e^{i\omega t}\vec{\epsilon}_{\vec{q},\nu}(R_z)] = \cos[\omega t]\mathrm{Re}[\vec{\epsilon}_{\vec{q},\nu}(R_z)] - \sin[\omega t]\mathrm{Im}[\vec{\epsilon}_{\vec{q},\nu}(R_z)]. \tag{28}$$

When the crystal has ''axial inversion symmetry,''[49] $\mathrm{Re}[\vec{\epsilon}_{\vec{q},\nu}(R_z)]$ and $\mathrm{Im}[\vec{\epsilon}_{\vec{q},\nu}(R_z)]$ are perpendicular to each other and one of them is perpendicular to the surface (thus the other is parallel to the surface). We thus have a parabolic orbit with the main axes as the real and imaginary part of the polarization vector. In general the so called surface Rayleigh is polarized mainly in the direction perpendicular to the surface and the longitudinal surface mode mainly in the direction of the momentum. The calculated phonon dispersion plots are given in Figs. 2 and 3, for Cu(111) and Al(100), respectively.

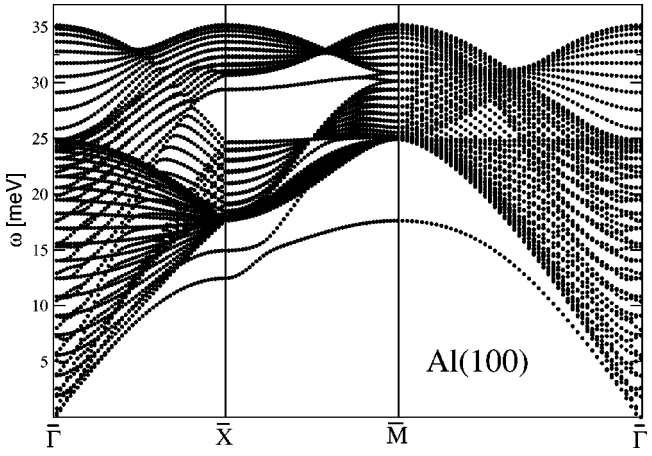

FIG. 3. Phonon dispersion of the Al(100) surface presented in the principal directions of the surface Brillouin zone.

IV. CALCULATION RESULTS AND DISCUSSION

In this section we analyze the dependence of obtained results on the electronic screening. Furthermore, we perform a detailed analysis of the different perturbation pictures, Bloch and Fröhlich, for the case of the intraband scattering. Finally we present the calculation results based on the theory discussed in the preceding section. We resolve the different contributions to the Eliashberg function, lifetime broadening, and the electron-phonon coupling parameter λ for the surface state of Al(100), Ag(111), Cu(111), and Au(111). While Au(111), Ag(111), and Cu(111) present a surface hole state well localized within a few layers at the surface, the Al(100) surface state decays very slowly into the bulk as this surface state located in a relatively narrow energy gap lies very close to the bottom of the band gap. Schematic drawings of band structure, with the surface state band, of the three metals surfaces can be seen in Figs. 8, 12, and 14. Due to the deep penetration of the Al(100) surface state into the bulk, the *e-p* coupling is similar to what is found in bulk Al. In general we find for the three systems that the interband contribution dominates and the intraband contribution is small ($<10\%$).

A. Screening

The screening of the bare ion potential is crucial for a realistic calculation of the electron-phonon matrix element. The ionic motion creates an additional charge distribution (with respect to the unperturbed situation) and the electron gas screens almost instantaneously this ''change'' in the potential.

Most of the results presented in this paper are calculated using the simple static Thomas-Fermi dielectric function. In this section we show that this approach gives similar results as the ones obtained from a more elaborate RPA treatment. The main advantage of the Thomas-Fermi theory is that it allows one to work with analytic formulas. However, this approach does not take into account the surface effects. The electron-phonon interaction is reasonably local around ionic positions and thus we find that the errors introduced are small. The static RPA dielectric function is defined as

$$\epsilon^{-1}_{RPA}(r-r') = \delta(r-r') + \int dr_1 v_c(r'-r_1)\chi_{RPA}(r_1,r'), \tag{29}$$

where v_c is the bare Coulomb potential,

$$\chi_{RPA}(r,r') = \chi^0(r,r') + \int dr_1 \int dr_2 \chi^0(r,r_1) \times v_c(r_1-r_2)\chi_{RPA}(r_2,r'), \tag{30}$$

and where $\chi^0(r,r')$ is the static density-density response function of a noninteracting electron gas,

$$\chi^0(r,r') = 2\sum_{i,j} \frac{\theta(E_F-\epsilon_i)-\theta(E_F-\epsilon_j)}{\epsilon_i-\epsilon_j+i\eta} \times \psi_i(r)\psi_j^*(r)\psi_j(r')\psi_i^*(r'). \tag{31}$$

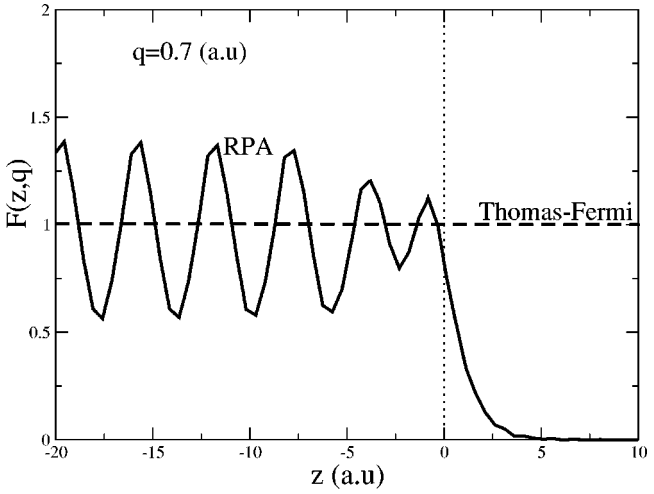

FIG. 4. Comparison between RPA (solid line) and Thomas-Fermi (dashed line) dielectric functions in the Cu(111) surface. $F(z,q)$, defined in Eq. (36), calculated for $q \approx q_F$.

$\psi_i(r)$ are a set of unperturbed single-particle wave functions of energy ϵ_i. We calculate these wave functions with the model potential described in Sec. III. As this potential is constant in a plane parallel to the surface, we use the 2D Fourier transform for all quantities entering Eq. (29), that leads to

$$\epsilon^{-1}_{RPA}(z-z',q) = \delta(z-z') + \int dz_1 v_c(z-z_1,q) \times \chi_{RPA}(z_1,z',q), \tag{32}$$

where $v_c(z'-z_1,q)$ refers to the 2D Fourier transform of the bare Coulomb potential. The 2D Fourier transform of the Thomas-Fermi dielectric function is obtained by back Fourier transforming the 3D dielectric function with respect to q_z. We then obtain

$$\epsilon^{-1}_{TF}(z-z',q) = \delta(z-z') - \frac{q^2_{TF} e^{-\sqrt{q^2+q^2_{TF}}|z-z'|}}{2\sqrt{q^2+q^2_{TF}}}. \tag{33}$$

In order to compare the RPA and Thomas-Fermi screening it is reasonable to compare the product $v_c \cdot \chi_{RPA}$ with the second term of the right-hand side of Eq. (33). For this purpose we define the following quantities:

$$\overline{v_c \chi_{RPA}(z)} \equiv \int dz' \int dz_1 v_c(z'-z_1,q) \chi_{RPA}(z_1,z',q) \tag{34}$$

for the RPA dielectric approach, and

$$\overline{v_c \chi_{TF}} \equiv \int dz' \frac{q^2_{TF} e^{-\sqrt{q^2+q^2_{TF}}|z-z'|}}{2\sqrt{q^2+q^2_{TF}}} = \frac{q^2_{TF}}{q^2_{TF}+q^2} \tag{35}$$

for the TF dielectric function. Thus we measure the relative difference dividing Eq. (34) by Eq. (35),

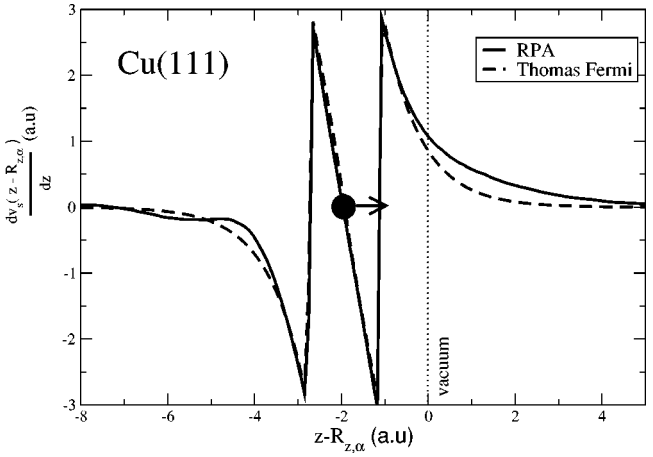

FIG. 5. Derivative, with respect to the z coordinate, of the 2D Fourier transform of the screened Ashcroft pseudopotential. Applying the RPA dielectric function (solid line) and Thomas-Fermi dielectric function (dashed line).

$$F(z,q) \equiv \frac{\overline{v_c \chi_{RPA}(z)}}{\overline{v_c \chi_{TF}}}. \tag{36}$$

In Fig. 4 we plot this ratio for $q=0.7$ (a.u.) in the surface region of Cu(111). This value of the momentum transfer is close to the Fermi momentum. Note that in this figure that the RPA result (solid line) oscillates around the value given by the Thomas-Fermi theory (dashed line).

In the calculation of the e-p coupling function g, given by Eqs. (10) and (11), the 2D Fourier transform of the gradient of the screened potential enters. The gradient of the screened potential reads

$$\vec{\nabla}_{\vec{R}_\alpha} v_s(\vec{r}-\vec{R}_\alpha)|_{\vec{R}^0_\alpha} = -\vec{\nabla}_{\vec{r}} v_s(\vec{r}-\vec{R}^0_\alpha), \tag{37}$$

where v_s is the screened pseudopotential and the 2D Fourier transform of Eq. (37):

$$F_{2D}[\vec{\nabla} v_s(\vec{r}-\vec{R}_\alpha)] \equiv \left(-i\vec{q} \cdot v_s(\vec{q},z-R_{\alpha,z}) + \hat{z} \cdot \frac{d}{dz} v_s(\vec{q},z-R_{\alpha,z}) \right) e^{i\vec{q}\cdot\vec{R}_\alpha}. \tag{38}$$

Let us compare the RPA and Thomas-Fermi screened deformation potential. With the Ashcroft pseudopotential (see Appendix B) as bare potential, we obtain the result shown in Fig. 5, where we plot both results (applying TF and RPA screenings) for the second term of Eq. (38) for the last atomic layer of the Cu(111) surface. The difference is small except the region beyond the surface where the RPA screening is slightly less strong. The reason for this is that the RPA screening actually takes into account the reduced electron density on the vacuum side of the surface layer.

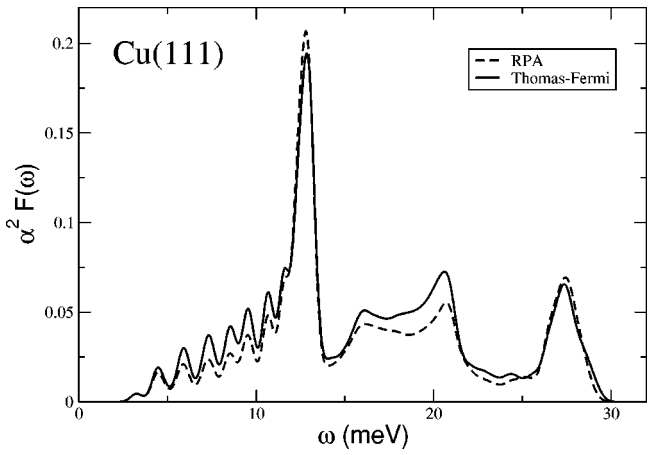

FIG. 6. Eliashberg function for the surface state of Cu(111) in the $\bar{\Gamma}$ point. Ashcroft pseudopotential screened by the RPA dielectric function (solid line) and the Thomas-Fermi dielectric function (dashed line).

Finally, the Eliashberg function is calculated for the Cu(111) surface state at the $\bar{\Gamma}$ point, making use of the Thomas-Fermi and RPA dielectric functions. The result is shown in Fig. 6. The agreement between both types of screening is reasonable and justifies the subsequent use of the Thomas-Fermi dielectric function.

B. Bloch and Fröhlich perturbation picture

In this subsection we analyze qualitatively the small q problem appearing when calculating the intraband scattering considering the Bloch description. With the notation of Eq. (2), the unperturbed and perturbing Hamiltonians in the Bloch description would respectively be

$$H^0_{e,B}(\vec{r},[\vec{R}^0_\alpha]) = -\frac{\nabla^2}{2} + \sum_\alpha v_s(\vec{r}-\vec{R}^0_\alpha), \tag{39}$$

$$H_{e-p,B}(\vec{r},[\vec{R}_\alpha]) = \sum_\alpha [e^{-\vec{u}_\alpha \vec{\nabla}_R} - 1] v_s(\vec{r}-\vec{R}^0_\alpha). \tag{40}$$

Let us consider the initial and final states in the scattering process,

$$\psi_i = \phi_i(z) e^{-i\vec{x}\cdot\vec{k}}, \tag{41}$$

$$\psi_f = \phi_f(z) e^{-i\vec{x}\cdot(\vec{k}-\vec{q})}, \tag{42}$$

where $\vec{r}=(\vec{x},z)$. We further suppose that ϕ_i is localized in the surface region with an spatial extend Δz. Then we write the e-p coupling function in the Bloch description,

$$g_{2D,B} \equiv \langle \psi_f | H_{e-p,B} | \psi_i \rangle \sim \int dz \sum_\alpha \phi^*_f(z) \times [e^{(-i\vec{u}_{\parallel,\alpha}\cdot\vec{q} + u_{\perp,\alpha}\cdot\frac{d}{dz})} - 1] v_s(\vec{q}, z - R_{z,\alpha}) \phi_i(z), \tag{43}$$

where $\vec{u}_{\parallel,\alpha}$ denotes the component of the ion displacement vector parallel to the surface and $\vec{u}_{\perp,\alpha}$ the perpendicular component. Phonon modes in the limit $q\to 0$ and $\omega\to 0$ correspond to a nearly rigid translation of the crystal. This is easy to understand as the $q\to 0$ limit brings us to a one-dimensional problem (direction perpendicular to the surface) and $\omega\to 0$ means physically an infinitely slowly moving crystal in this direction with all ions moving nearly in phase. In this limit we have

$$\vec{u}_{\perp,\alpha} \sim \sqrt{\frac{1}{M\omega}} \cdot e^{i\cdot(\omega/c)\cdot R_{z,\alpha}}, \quad (q\to 0, \omega\to 0), \tag{44}$$

where c is a typical phonon velocity. We now consider the final-state wave function in Eq. (42) given by ψ_f. We expand Eq. (40) around the equilibrium ion positions,

$$g_{2D,B} \simeq \int dz \left[\sum_\alpha \phi^*_f(z) \left(-i\vec{u}_{\parallel,\alpha}\cdot\vec{q} + u_{\perp,\alpha}\frac{d}{dz} \right) \times v_s(\vec{q}, z - R_{z,\alpha}) \phi_i(z) \right]. \tag{45}$$

Taking into account Eq. (44) and the fact that in the limit $q\to 0$, only intraband scattering can take place ($f=i$), a partial integration yields in the limit $q\to 0$, $\omega\to 0$

$$g_{2D,B} \simeq \sum_\alpha u_{\perp,\alpha} \int dz \left(\frac{d}{dz} [\phi^*_i(z)\phi_i(z)] v_s(\vec{q}, z - R_{z,\alpha}) \right). \tag{46}$$

If we now consider that the surface state has an spatial extend Δz, we can make use of the following approximation for the squared amplitude of the wave function:

$$|\phi_i(z)|^2 \sim \frac{e^{\frac{z}{\Delta z}}}{\Delta z}\theta(-z), \quad \frac{\partial}{\partial z}|\phi_i(z)|^2 \sim \frac{e^{\frac{z}{\Delta z}}}{\Delta z^2}\theta(-z). \tag{47}$$

Furthermore, we have the Thomas-Fermi screened potential in the limit $q\to 0$ (see Appendix B)

$$v_s(0, z - R_{z,\alpha}) < \frac{e^{-q_{TF}\cdot|z-R_{z,\alpha}|}}{q_{TF}}. \tag{48}$$

Analyzing the contribution from the first layer, and multiplying by the factor $(\Delta z)/a_0$ (the number of layers within Δz, a_0 being the distance between layers), one easily obtains

$$g_{2D,B} \sim \frac{1}{\sqrt{M\cdot\omega}} \cdot \frac{1}{a_0 \Delta z \left[\frac{q_{TF}}{\Delta z} + q^2_{TF} \right]}. \tag{49}$$

This result tells us that the more confined the surface state is and the smaller the phonon energy, the stronger is the interaction in the Bloch description. Finally we get the estimated lifetime broadening from Eq. (A20) in the limit $\omega \to 0$,

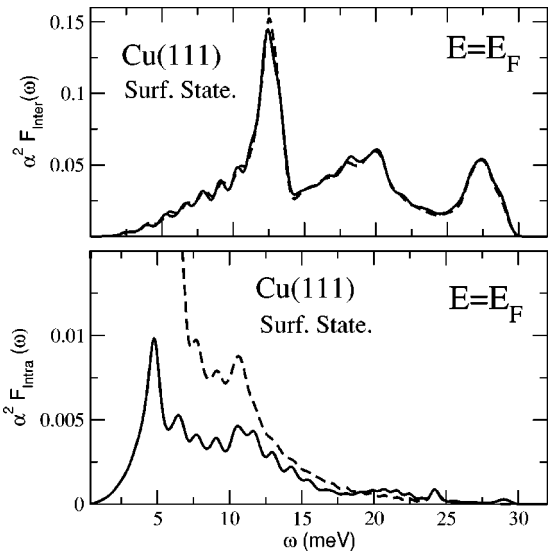

FIG. 7. The top panel shows the interband contribution to the Eliashberg function for the surface state of Cu(111) at the Fermi level in the Bloch description (dashed line) and in the Fröhlich description (solid line). In the bottom panel we show the intraband contribution in the Bloch description (dashed line) and in the Fröhlich description (solid line).

$$\Gamma(\epsilon_{i,\vec{k}_i}) \sim \int_0^\infty [\alpha^2 F^E_{i,\vec{k}_i}(\omega) + \alpha^2 F^A_{i,\vec{k}_i}(\omega)] \cdot \frac{k_B T}{\omega} d\omega. \quad (50)$$

From Eqs. (8), (9), and (49) we find

$$\Gamma(\epsilon_{i,\vec{k}_i}) \sim \int_0^{\omega_m} \frac{1}{\omega^2} d\omega, \quad (51)$$

which is diverging. We conclude that the Bloch description is not appropriate in the small q limit, giving an unphysical divergent result.

Rahman and Mills[50] found this problem in a related work. Using a Green-function formalism, they treated the electron Green function with a finite damping, giving rise to a nondiverging result. However, with this procedure one needs an estimation of the damping (broadening) in order to calculate the lifetime (inverse of the broadening). We find the Fröhlich description to be a more physically transparent way to remove this spurious divergence.

The analysis based on the Fröhlich description is very similar to the preceding for the Bloch description, but now we must replace $\vec{u}_\alpha$ by $\vec{u}_\alpha - \vec{U}$. It is obvious that this difference is zero for a rigid translation of the crystal or tend to zero for low-energy phonons. The relative phase difference between the polarization vectors in the Δz area close to the surface is

$$\Delta\phi \approx \frac{\Delta z \cdot \omega}{c} (\vec{q} \to 0, \omega \to 0), \quad (52)$$

we thus have

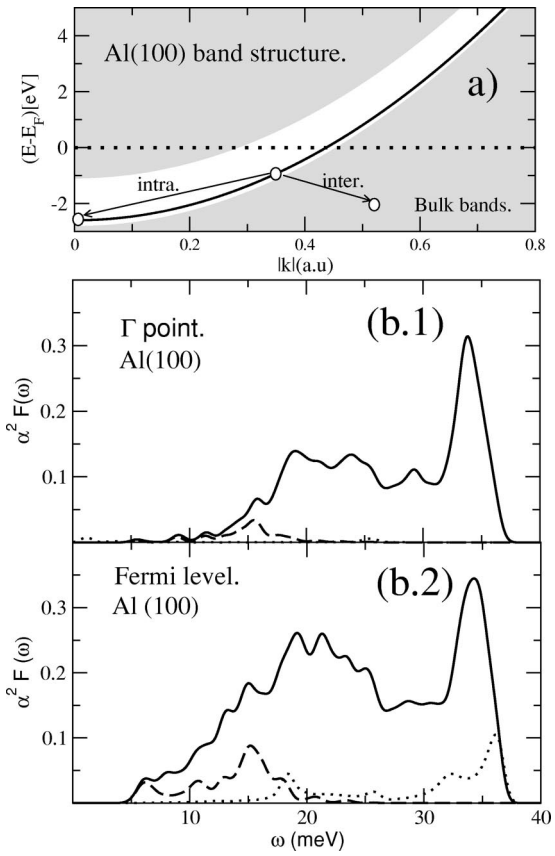

FIG. 8. (a) Schematic drawing of the band structure of the Al(100) surface with the surface-state band (solid line) and surface projected bulk bands (shaded region). (b) Eliashberg function resolved in terms of interband scattering (solid line), intraband scattering (dotted line), and surface Rayleigh phonon induced scattering (dashed line). In panels (b.1) and (b.2), the calculated result at the Γ point and at the Fermi level are shown, respectively.

$$|\vec{u}_\alpha - \vec{U}| \sim \frac{1}{\sqrt{M \cdot \omega}} \cdot |(e^{i\Delta\phi} - 1)| \sim \frac{1}{\sqrt{M \cdot \omega}} \cdot \frac{\Delta z \cdot \omega}{c}. \quad (53)$$

The e-p coupling function is then

$$g_{2D,F} \equiv \langle \psi_f | H_{e-p,F} | \psi_i \rangle \sim \frac{1}{\sqrt{M \cdot \omega}} \cdot \frac{1}{\Delta z^2 \left[\frac{q_{TF}}{\Delta z} + q_{TF}^2 \right]} \frac{\Delta z \cdot \omega}{c} \left(\frac{\Delta z}{a_0} \right) = \sqrt{\frac{\omega}{M}} \cdot \frac{1}{\frac{q_{TF}}{\Delta z} + q_{TF}^2} \frac{1}{c \cdot a_0}, \quad (54)$$

which gives an Eliashberg function $\alpha^2 F(\omega) \sim \omega$ in the limit $\omega \to 0$. Thus, according to Eq. (50), the lifetime broadening Γ converges and a finite result is obtained.

From this qualitative analysis we have shown that the Fröhlich perturbation description is appropriate in order to calculate the phonon induced intraband scattering. To illus-

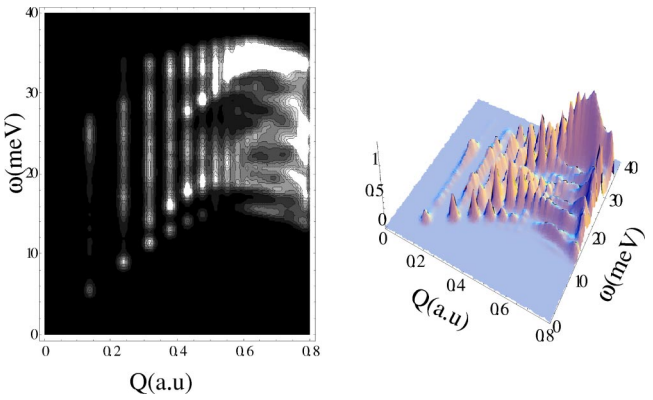

FIG. 9. Scattering probability with an energy ω and momentum modulus loss Q [defined in Eq. (17)], respectively, for the Al(100) surface state in the $\bar{\Gamma}$ point at zero temperature. Note that the scattering probability is distributed mainly in the bulk phonon mode phase space area (compare with Fig. 3).

trate this we show in Fig. 7 the calculated Eliashberg function for the surface state of Cu(111) in the Bloch and the Fröhlich picture for the interband (top panel) and intraband contribution (bottom panel). For the interband contribution both approaches completely agree, but for the intraband contribution it is clearly shown how the Bloch description based Eliashberg function diverges for small ω.

We conclude that the definition of the unperturbed wave function (solution of the rigid lattice in the Bloch description) is not appropriate for this kind of problem. The divergence in the Bloch description is related to the dimensionality of the problem and it is absent in the bulk 3D case. To illustrate this fact, let us consider the *e-p* coupling matrix element in the Bloch picture applying 3D plane waves for the electron wave functions. The matrix element is simply the 3D Fourier transform of the perturbation part of the Hamiltonian,

$$g_{3D,B} \sim \langle e^{-i\vec{k}\cdot\vec{r}} | H_{e-p,Blo} | e^{-i(\vec{k}-\vec{q})\cdot\vec{r}} \rangle$$

$$\sim \sum_{\alpha} [e^{i\vec{u}_{\alpha}\cdot\vec{q}} - 1] v_s(\vec{q}), \tag{55}$$

where $v_s(\vec{q})$ is the Fourier transform for the screened pseudopotential. In three dimensions only longitudinal phonons contributes and in the long-wavelength limit ($q \rightarrow 0$) we have $\omega = cq$. From Eq. (55) we obtain

$$g_{3D,B} \sim \sqrt{\frac{\omega}{M \cdot c^2}}, \quad (q \rightarrow 0, \omega \rightarrow 0). \tag{56}$$

This gives a similar result as for the matrix element obtained for 2D states in Fröhlich description [Eq. (54)], and thus the divergence disappears also in this case.

C. Surface states on Al(100), Ag(111), Cu(111), and Au(111)

In this subsection we present the calculation results for the lifetime broadening and *e-p* coupling parameter λ. The

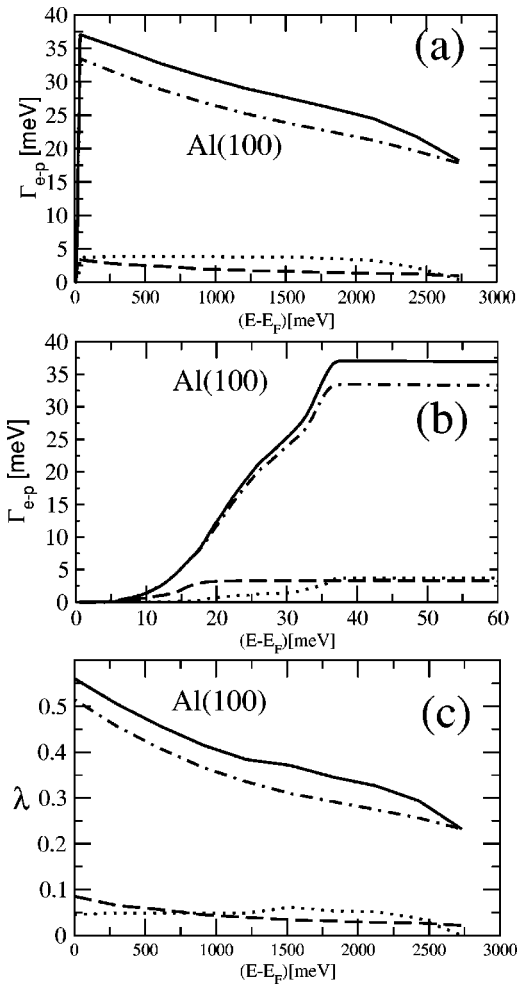

FIG. 10. (a) The $T=0$ phonon induced lifetime broadening versus binding energy for the surface state of Al(100). All binding energies between zero at the Fermi level and the maximum value in the $\bar{\Gamma}$ point are shown. The contribution from the interband scattering (dashed-dotted line), intraband scattering (dotted line), Rayleigh phonon induced scattering (dashed line), and the total broadening (solid line). (b) A blowup of panel (a) close to E_F. (c) The *e-p* coupling parameter λ versus binding energy. The total quantity (solid line) is resolved in contributions from the interband scattering (solid line), intraband scattering (dotted line), Rayleigh phonon induced scattering (dashed line), and the interband scattering (dashed-dotted line).

major part of our analysis is based on examining the different contributions to the spectral Eliashberg function, such as intra- and interband scattering ones, and surface and bulk phonons contributions. To compare with experiment we also show the temperature and hole binding energy dependence of the lifetime broadening and the binding energy dependence of the λ parameter. We have previously presented a minor part of these results for the $\bar{\Gamma}$ surface-states of Cu(111) and Ag(111).[31] Now we also include some calculation results for Au(111) and an analysis of the $\bar{\Gamma}$ surface state on Al(100), which is qualitatively different, having a surface state band deeper in energy, located closer to the lower band gap edge.

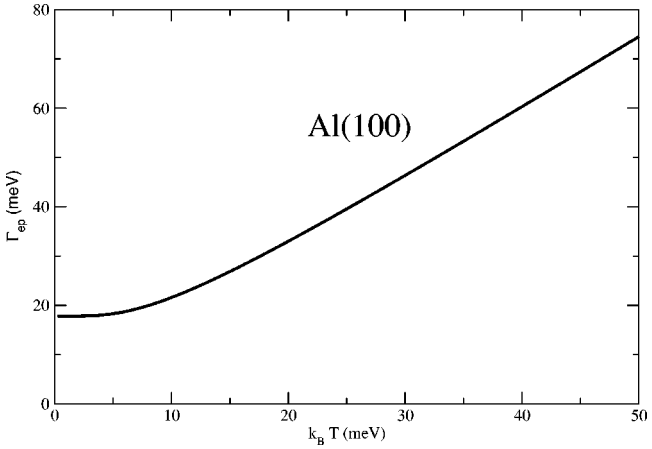

FIG. 11. The temperature dependence of the lifetime broadening Γ for the the surface state of Al(100) in the $\bar{\Gamma}$ point.

1. Al(100)

In Fig. 8 we show the different contributions to the Eliashberg function for the Al(100) surface hole state. The contribution from the surface Rayleigh phonon mode is small (dashed line), both at the $\bar{\Gamma}$ point and at the Fermi level. This result is consistent with the fact that the surface-state band is located near the lower band edge of the surface projected band gap and thus has a ''bulklike'' character. From Fig. 8 it is also clear that the interband scattering gives by far the most important contribution to the Eliashberg function. The intraband contribution is negligible in the $\bar{\Gamma}$ point but its importance is slightly increased upon approaching the Fermi level E_F.

In Fig. 9 we show the scattering probability for the Al(100) surface-state hole in the Γ point, losing an energy ω and momentum modulus Q [see Eq. (17)] in a phonon stimulated emission process. Most of the weight is concentrated near the maximum phonon energy ω_m, however, the scattering probability is quite spread out in the (ω,Q) space. Referring to Fig. 3, it is clearly seen that the contribution from the surface Rayleigh phonon mode is very small and that the bulk phonon modes are more important.

The lifetime broadening due to the *e-p* coupling will depend on where in the surface-state band the hole is created. In particular the energy dependence of the broadening is strong when the binding-energy is less than the maximum phonon frequency. The top panel of Fig. 10 gives the binding energy dependence of the lifetime broadening and the middle panel of Fig. 10 shows a blowup near the Fermi level. This general binding-energy dependence is easy to understand. If we consider the case when $T=0$, no phonon absorption occur. The zero value of Γ for zero binding energy (hole at the Fermi level) is due to the fact that no electrons can scatter into the hole. When the hole binding increases increase from zero to the maximum phonon energy, gradually more and more phonons are energetically available, determined by the integration of the Eliashberg function up to the actual binding energy. As the binding energy exceeds the maximum phonon energy, Γ_{e-p} more or less saturates. However, a decrease of Γ_{e-p} is seen in the top panel of Fig. 10 when the

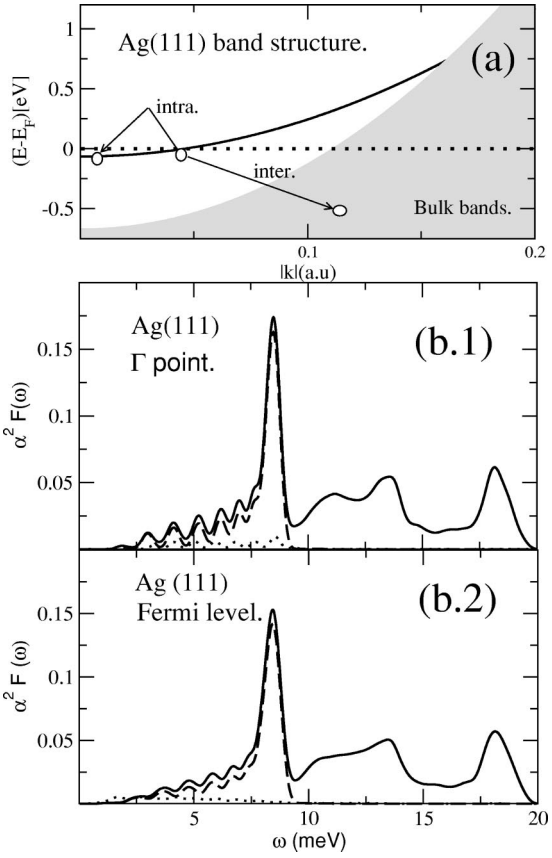

FIG. 12. (a) Schematic drawing of the band structure of the Ag(111) surface with the surface-state band (solid line) and surface projected bulk bands (shaded region). (b) Eliashberg function resolved in terms of interband scattering (solid line), intraband scattering (dotted line), and surface Rayleigh phonon induced scattering (dashed line). In panels (b.1) and (b.2), the calculated result at the Γ point and at the Fermi level are shown, respectively.

binding energy increases from the maximum phonon energy to the maximum binding energy in the $\bar{\Gamma}$ point. This decrease is due to the relatively deep surface-state band [in comparison with Cu(111) and Ag(111) discussed later on]. When moving from the Fermi level to the $\bar{\Gamma}$ point the mean momentum transfer decreases and thus the weaker is the matrix element [Eq. (38)].

The surface Rayleigh phonon mode contribution (dashed line in top and middle panel of Fig. 10) represents only about the 10% of the total broadening (solid line) close to the Fermi level and decreases substantially moving to the maximum binding energy ($\bar{\Gamma}$ point). Up to a binding energy corresponding to the maximum phonon energy, the intraband contribution increases and saturates at about $\sim$10% of the total.

The λ parameter, given by the first reciprocal moment of the Eliashberg function [see Eq. (16)], is shown in the lower panel in Fig. 10. The decrease of λ with increasing binding energy is explained by the same argument as above for Γ. Only about the 6% of the Al(100) wave function is located on the vacuum side of the surface layer. This explains why the λ values reported here are comparable to results from

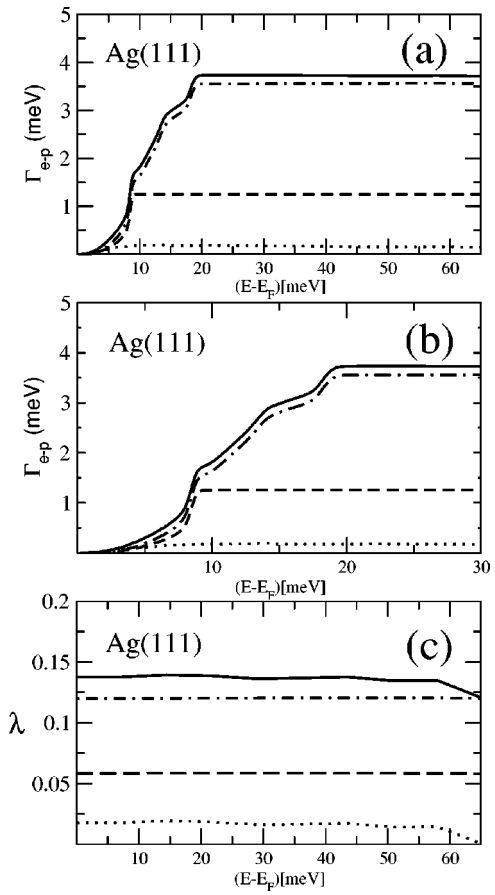

FIG. 13. (a) The $T=0$ phonon induced lifetime broadening versus binding energy for the surface state of Ag(111). All binding energies between zero at the Fermi level and the maximum value in the $\bar{\Gamma}$ point is shown. The contribution from the interband scattering (dashed-dotted line), intraband scattering (dotted line), Rayleigh phonon induced scattering (dashed line), and the total broadening (solid line). (b) A blowup of panel (a) close to E_F. (c) The *e-p* coupling parameter λ versus binding energy. The total quantity (solid line) is resolved in contributions from the interband scattering (solid line), intraband scattering (dotted line), Rayleigh phonon induced scattering (dashed line), and the interband scattering (dashed-dotted line).

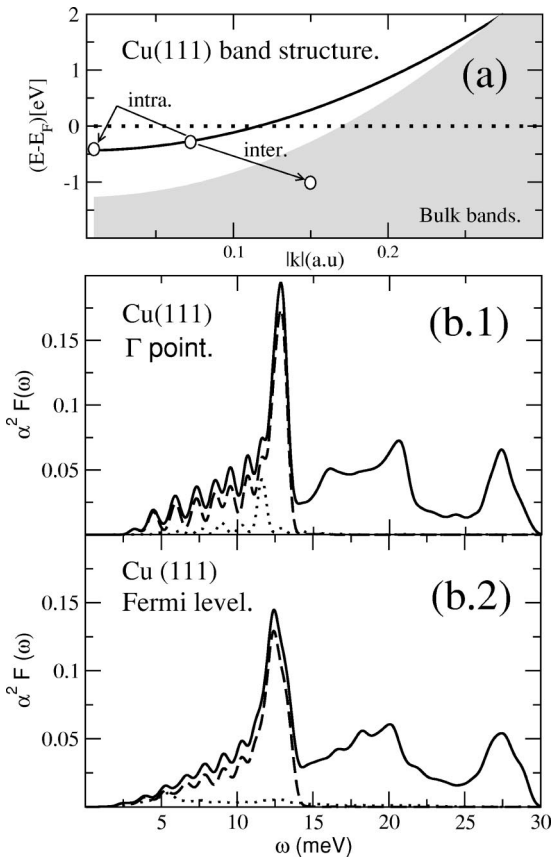

FIG. 14. (a) Schematic drawing of the band structure of the Cu(111) surface with the surface-state band (solid line) and surface projected bulk bands (shaded region). (b) Eliashberg function resolved in terms of interband scattering (solid line), intraband scattering (dotted line), and surface Rayleigh phonon induced scattering (dashed line). In panels (b.1) and (b.2), the calculated result at the Γ point and at the Fermi level are shown, respectively.

previous bulk calculations. In the work by S. Y. Savrasov and D. Y. Savrasov[51] a value of $\lambda=0.44$ is reported for bulk Al which is comparable to our $\lambda\sim0.55$ at E_F.

The lifetime broadening as a function of temperature for the surface state of Al(100) in the $\bar{\Gamma}$ point is shown in Fig. 11. At zero temperature there are no phonons excited and the finite lifetime broadening is due to phonon emission scattering processes. For temperatures $k_BT\gg\omega_m$, where ω_m is the maximum phonon frequency we see the linear T dependence with a slope determined by λ [see Eq. (16)].

2. Ag(111), Cu(111), and Au(111)

Qualitatively, the results for Ag(111), Cu(111), and Au(111) are similar. All the surface-state bands are shallow, giving a maximum hole binding energy (in the $\bar{\Gamma}$ point) of 60, 440, and 500 meV, respectively. A schematic picture of the surface band structure for Ag(111) and Cu(111) is given in Figs. 12(a) and 14(a). In both cases, the surface-state band is located well inside the surface projected band gap. Thus the wave function of the surface state is more localized at the surface in comparison with the case of Al(100) discussed above. We find that for all these surfaces the surface state is localized within the top $\sim3-5$ layers. This means that the physics of the electron-phonon coupling for Ag(111), Cu(111), and Au(111) surface states should be sensitive to surface phonon modes.

A direct consequence of the small hole binding energy of the surface states of Ag(111), Cu(111), and Au(111) is the weak energy dependence of the integrated quantities Γ and λ for binding energies exceeding the maximum phonon frequency. This is seen in Figs. 13 and 16. The increase of Γ with binding energy from zero to the maximum phonon energy reflects as in the case of Al(100), inclusion of more possible scattering events, corresponding to a gradually increased upper limit of the integration of the Eliashberg functions [see Figs. 12(b), 12(c), 14(b), and 14(c)].

It is interesting to note that the Rayleigh mode dominates the contribution to the low-energy part of the calculated spectral Eliashberg function ($\omega<\omega_{max}/3$). Within this small binding energy range the interaction with the Rayleigh mode

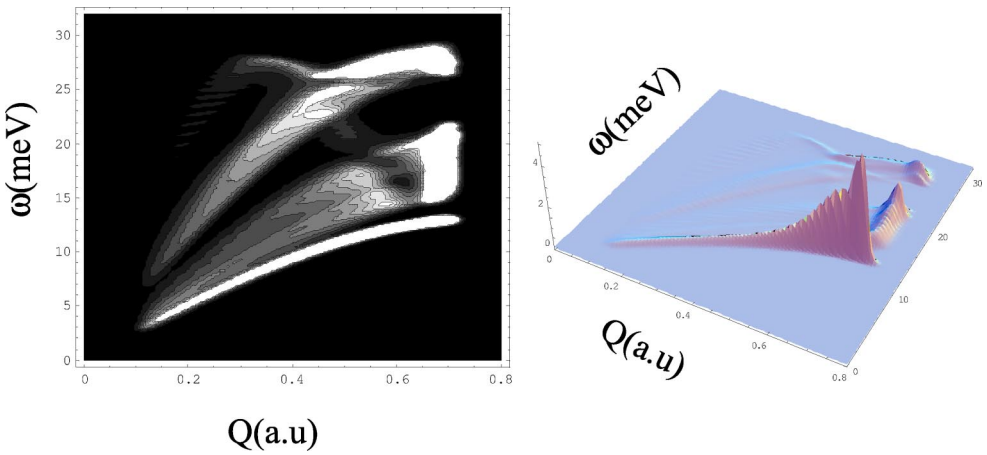

FIG. 15. Scattering probability with an energy ω and momentum modulus loss Q [defined in Eq. (17)], respectively, for the Cu(111) surface state in the $\bar{\Gamma}$ point at zero temperature. Note that most of the scattering probability is concentrated around the surface Rayleigh dispersion curve, decaying in strength as the scattering momentum is smaller (compare with Fig. 2). The case of Ag(111) is similar.

dominates. This is then reflected in the lifetime broadening Γ shown in Figs. 13(b) and 16(b). We find that the Rayleigh mode contribution to the level broadening in the range E_F ($\omega_{BE} < \omega_m/3$) gives about 90% for the Ag(111) and Cu(111) surface states.

The intraband contribution is very small for both Ag(111) and Cu(111). In Figs. 12(b), 12(c), 14(b), and 14(c) the intraband contribution to the Eliashberg function is shown (dotted line).

In Fig. 15 we show the spectral Eliashberg function defined in Eq. (17) for the surface hole state in the $\bar{\Gamma}$ point of Cu(111). The intensity of the peaks is proportional to the probability for the hole to scatter at a given energy and momentum modulus. We can understand this figure by comparing with the phonon dispersions of Cu(111) in Fig. 2. Figure 15 clearly reveals the importance of the surface Rayleigh phonon mode. The surface phonon mode amplitude has the behavior $u_z \sim e^{-|q|\cdot R_z}$, where R_z is the layer distance from the surface. Surface phonon modes have an increased bulk penetration the larger the wavelength is (small q) and thus the relative interaction with the surface state decreases for small q. This is manifested in Fig. 15 as the contribution from the Rayleigh mode has an exponential like decay going to the small momentum region of the Rayleigh mode. The main part of the intraband scattering is mediated by the surface Rayleigh mode, as both the hole and the this phonon mode are localizated in the surface area.

The λ parameter dependence with binding energy is shown in Figs. 13(c) and 16(c) for Ag(111) and Cu(111) surface states, respectively. In both cases intraband contribution represent about the 10% of the total λ value. The reason why the relative weight of the intraband contribution in Ag(111) and Cu(111) is larger for the λ parameter, than for the broadening, is that the main contribution to the intraband scattering comes from the Rayleigh mode. Furthermore, these scattering events involve small energy transferences (small ω) and thus favor a large λ value [see Eq. (16)].

The temperature dependence of the lifetime broadening of the surface states in the $\bar{\Gamma}$ point of the surface Brillouin zone of the three noble metal surfaces is shown in Fig. 17. The slightly steeper slope for Cu(111) reflects the larger λ parameter. In a recent publication[31] we have compared the temperature dependence of the broadening to experimental high-resolution PES data in Ag(111) and Cu(111), for the hole in the $\bar{\Gamma}$ point. Taken into account the e-e scattering contribution to the broadening we find that the agreement with experiment is excellent for all noble metal surfaces studied.

V. SUMMARY AND CONCLUSIONS

We have presented an analysis of the phonon induced contribution to the lifetime broadening Γ of surface band states. The aim of this work is to understand the decay of surface states through the electron-phonon interaction. We give the details of lifetime broadening due to the electron-phonon coupling for the surface band on Al(100), Ag(111), Cu(111), and Au(111) and the role of surface phonons and the electronic screening are clarified. We resolve the contribution to Γ in terms of intraband and interband scattering and we present a general approach how to avoid the unphysical divergence appearing when calculating the contribution from intraband scattering.

With a correct treatment of the intraband scattering we have shown that for the systems we have studied the contributions to the lifetime broadening from interband scattering dominate completely over the contributions from intraband scattering.

Concerning the calculated lifetime broadening, Γ and the e-p coupling parameter λ, these quantities are determined by the e-p matrix elements. There are several components that determine the magnitude of these matrix elements, the overlap between initial electron state, phonon modes, screened deformation potential, and final electron state. In addition the strength of the deformation potential is of importance.

First of all, the results for the surface states on Ag(111), Cu(111), and Au(111) are qualitatively the same since on these systems the surface state band is shallow and far from the band-gap edges. The surface-state band on Al(100) is

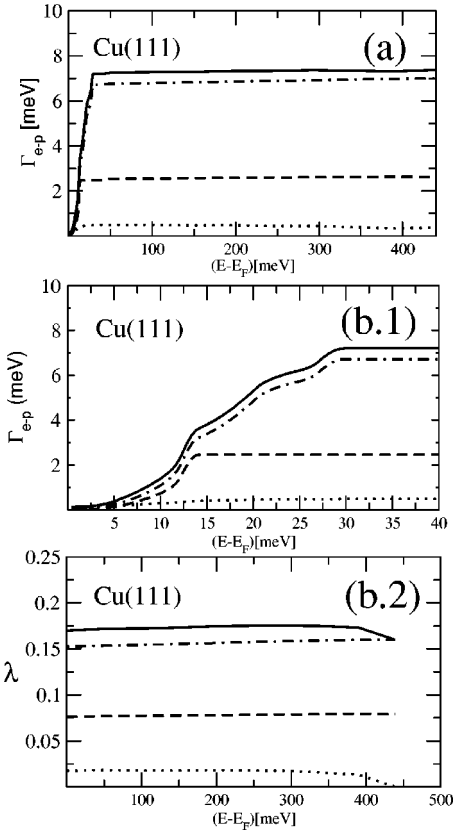

FIG. 16. (a) The $T=0$ phonon induced lifetime broadening versus binding energy for the surface state of Cu(111). All binding energies between zero at the Fermi level and the maximum value in the $\bar{\Gamma}$ point is shown. The contribution from the interband scattering (dashed-dotted line), intraband scattering (dotted line), Rayleigh phonon induced scattering (dashed line), and total broadening. (b) A blowup of panel (a) close to E_F. (c) The *e-p* coupling parameter λ versus binding energy. The total quantity (solid line) is resolved in contributions from the interband scattering (solid line), intraband scattering (dotted line), Rayleigh phonon induced scattering (dashed line), and the interband scattering (dashed-dotted line).

deeper in energy and appears very close to the lower band-gap edge, which results in a more extended wave functions into the bulk. This means that the overlap with final bulk states increases. As a consequence, we found that for Al(100) the most important phonon modes are bulklike ones and not localized in the surface layers. On the other hand, the screened deformation potential turns out to be substantially stronger in comparison with Ag, Au, and Cu. In the case of Ag, Cu, and Au the *bare* pseudopotentials have the charge $Z = +1$, while for Al, $Z = +3$. Even if there are more electrons to screen the Al pseudopotential it turns out that the screened deformation potential is strong. This is the main reason why Γ is an order of magnitude larger for Al(100) than for noble-metal surface states.

The role of the surface Rayleigh phonon mode is different when comparing Al(100) to the noble-metal surfaces. In the case of Al(100) the surface-state wave function extends further into the bulk and thus when calculating the *e-p* matrix elements, more of the bulk is sampled and the weight of bulk phonon modes becomes important. The result is that the Rayleigh mode gives less that 10% to both Γ and λ. However, for the noble-metal surfaces it completely dominates for binding energies smaller than the maximum Rayleigh mode energy (~90% of the total) and continues being important even for energies bigger than the Debye energy (~40% of the total). For the noble-metal surfaces nearly half of the value of the *e-p* coupling parameter λ is determined by the Rayleigh mode.

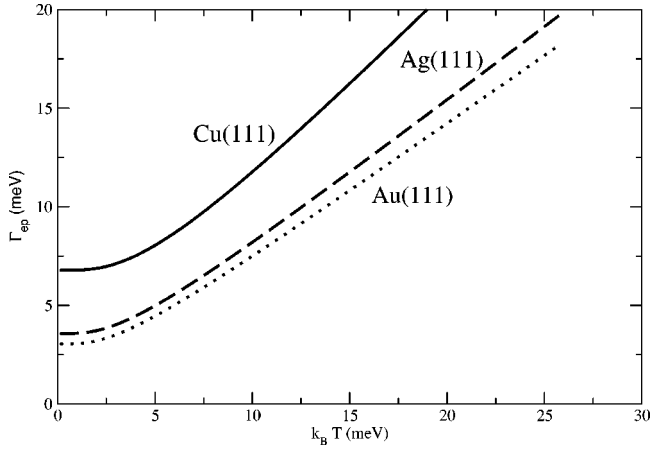

FIG. 17. The temperature dependence of the lifetime broadening Γ for the the surface state of Ag(111) and Cu(111) in the $\bar{\Gamma}$ point.

Finally we want to consider the *electron-electron* scattering contribution to the lifetime broadening in order to make a comparison with experimental data and to understand the relative importance of the here calculated, phonon induced contribution. In Table I we show the calculated phonon induced broadening Γ_{ep} for noble-metal surfaces states, and in order to compare with experimental data we also present the contribution from the *electron-electron* interaction Γ_{ee}. To compare with experiments we add the two contributions and obtain in these surfaces good agreement with very recent high quality photoemission results.[31]

For Al(100) a value $\Gamma_{ee}=131$ meV has been calculated at the $\bar{\Gamma}$ point within the same scheme as in Ref. 14 (a value of 67 meV has been evaluated in Ref. 52, however, without taking into account the surface screening). Thus the calculated total broadening of ~150 meV for Al(100) shows an apparent discrepancy with the available room-temperature photoemission data of broadening of 400–450 meV.[53,54] However, these results have been obtained in the 1980s by

TABLE I. Calculated electron-phonon (Γ_{ep}) and electron-electron (Γ_{ee}) contributions to the broadening, when the hole is at the $\bar{\Gamma}$ point. Γ_{exp} is the experimental width and λ the calculated electron-phonon coupling parameter.

	Γ_{ep} (meV)	Γ_{ee} (meV)	Γ_{expt} (meV)	λ
Ag(111)	3.7	2.0 [a]	6 [b]	0.12
Cu(111)	7.3	14 [a]	22 [b]	0.16
Au(111)	3.6	14 [a]	18 [a]	0.11

[a]Reference 14.
[b]Reference 31.

using significantly less clean samples and worse resolution compared to those achieved in 2000. The clear example of much more accurate measurement of today is the Cu(111) $s-p_z$ surface state. In 1983 Kevan obtained the broadening value of 55 meV at $\bar{\Gamma}$.[55] Recent scanning tunneling spectroscopy[14] and photoemission[24] low-temperature measurements gave a value of $\sim$20 meV, which is a factor of 2–3 smaller than the Kevan's result. It seems very desirable to measure the Al(100) surface-state broadening with modern photoemission resolution.

ACKNOWLEDGMENTS

We acknowledge financial support from the Basque Government, the Max Planck Research Award Funds, the Spanish Ministerio de Educación y Ciencia (MEC), the Basque Country University, and the Carl Tryggers Foundation.

APPENDIX A: DERIVATIONS OF PHONON INDUCED LIFETIME BROADENING

1. Calculation of the matrix element

If we expand Eq. (6) around $\vec{U}+\vec{R}_\alpha$ we obtain

$$H_{e-p,F}(\vec{r},[\vec{R}_\alpha])=\sum_\alpha\ (\vec{u}_\alpha-\vec{U})\cdot\vec{\nabla}_R v_s[\vec{r}-(\vec{R}^0_\alpha+\vec{U})]. \tag{A1}$$

In the harmonic approximation, the atomic displacement pattern for a phonon mode ν and momentum $\vec{q}$ is given by

$$\vec{u}_\alpha(R_\alpha)=\sqrt{\frac{1}{2M\omega^\nu_{\vec{q}}N_\parallel}}[a^+_{\vec{q},\nu}e^{-i\cdot\vec{q}\cdot\vec{R}_\alpha}\cdot\vec{\epsilon}_{\vec{q},\nu}(R_{\alpha,z})^\star + a_{\vec{q},\nu}e^{i\cdot\vec{q}\cdot\vec{R}_\alpha}\cdot\vec{\epsilon}_{\vec{q},\nu}(R_{\alpha,z})], \tag{A2}$$

where $\omega^\nu_{\vec{q}}$ and $\vec{\epsilon}_{\vec{q},\nu}(R_{\alpha,z})$ refer to the energy and the polarization vector in the lattice position $\vec{R}_\alpha$ which z component is $(R_{\alpha,z})$. $N_\parallel$ is the number of atomic positions considered in the atomic planes parallel to the surface within periodic boundary conditions.

Let us now define

$$\vec{\sigma}_{\vec{q},\nu}(R_{\alpha,z})=\vec{\epsilon}_{\vec{q},\nu}(R_{\alpha,z})-\sum_\beta^{\tilde{N}_z}\frac{\vec{\epsilon}_{\vec{q},\nu}(R_{\beta,z})}{\tilde{N}_z}, \tag{A3}$$

where β is the layer index and $\tilde{N}_z$ the number of layers in the surface where the surface state has an appreciable amplitude. The displacement in each atomic position $[\vec{u}_\alpha(R_\alpha)]$ with respect to the ''mean'' displacement $(\vec{U})$ can be written as

$$\vec{u}_\alpha(R_\alpha)-\vec{U}=\sum_{\vec{q},\nu}\ \sqrt{\frac{1}{2M\omega^\nu_{\vec{q}}N_\parallel}}\times[a^+_{\vec{q},\nu}e^{-i\cdot\vec{q}\cdot\vec{R}_\alpha}\cdot\vec{\sigma}_{\vec{q},\nu}(R_{\alpha,z})^\star + a_{\vec{q},\nu}e^{i\cdot\vec{q}\cdot\vec{R}_\alpha}\cdot\vec{\sigma}_{\vec{q},\nu}(R_{\alpha,z})]. \tag{A4}$$

For a phonon emission process, the initial and final states are written

$$\Phi_i=\psi_{k_i,i}(\vec{r}-\vec{U})\otimes|N^\nu_{\vec{q}}\rangle, \tag{A5}$$

$$\Phi_f=\psi_{k_f,i}(\vec{r}-\vec{U})\otimes|N^\nu_{\vec{q}}+1\rangle, \tag{A6}$$

where ψ and $|N\rangle$ represent, respectively, the electronic and phonon wave functions. For a phonon absorption process we should substitute $|N^\nu_{\vec{q}}+1\rangle$ by $|N^\nu_{\vec{q}}-1\rangle$.

The matrix elements corresponding to emission and absorption processes can be written as

$$\langle\Phi_i|H_{e-p}|\Phi_f\rangle_E=\sqrt{n_B(\omega_{\vec{q},\omega})+1}\cdot[g^{i,f}_{\vec{q},\nu}]^\star \times\sqrt{\frac{1}{\Omega}}\sum_{\vec{G}}\ \delta_{\vec{k}_i-\vec{k}_f,\vec{q}+\vec{G}}, \tag{A7}$$

$$\langle\Phi_i|H_{e-p}|\Phi_f\rangle_A=\sqrt{n_B(\omega_{\vec{q},\omega})}\cdot[g^{i,f}_{\vec{q},\nu}]^\star \times\sqrt{\frac{1}{\Omega}}\sum_{\vec{G}}\ \delta_{\vec{k}_i-\vec{k}_f,-\vec{q}+\vec{G}}, \tag{A8}$$

where Ω is the area considered parallel to the surface ($\Omega=\Omega_0 N_\parallel$, where Ω_0 is the area corresponding to each atomic position). The electronic part of the matrix element is

$$g^{i,f}_{\vec{q},\nu}\equiv\sqrt{\frac{1}{2M\omega_{\vec{q},\nu}\Omega_0}}\int dz\,\phi_i(z)G_{\vec{q}}(z)\phi_f(z), \tag{A9}$$

where

$$G_{\vec{q}}(z)=\sum_{R_{\alpha,z}}\vec{\sigma}_{\vec{q},\nu}(R_{\alpha,z})\cdot e^{i\vec{q}\cdot\vec{c}}\cdot F_{2D}[\vec{\nabla}v_s(\vec{r}-\vec{R}_\alpha)]. \tag{A10}$$

In the integration of the electron coordinate $\vec{r}$ a change of variable $\vec{r}\rightarrow\vec{r}'+\vec{U}$ can be done. In this way, the only effect of the mean displacement $\vec{U}$ in the calculation of the matrix element appears in the amplitude of the atomic motions relative to $\vec{U}$ [as in Eq. (A4)]. The $\vec{c}$ is the vector translating all the atoms on one layer to the same parallel components as the layer below. We have used the fact that

$$\sum_{R_{\alpha,\parallel}}e^{-i(\vec{k}_i-\vec{k}_f\pm\vec{q})\cdot\vec{R}_{\alpha,\parallel}}=N_\parallel\sum_{\vec{G}}\ \delta_{\vec{k}_i-\vec{k}_f,\mp\vec{q}+\vec{G}} \tag{A11}$$

and also

$$F_{2D}[\vec{\nabla}v_s(\vec{r}-\vec{R}_\alpha)] \equiv\left(-i\vec{q}\cdot v_s(\vec{q},z-R_{\alpha,z})+\hat{z}\cdot\frac{d}{dz}v_s(\vec{q},z-R_{\alpha,z})\right)e^{i\vec{q}\cdot\vec{R}_\alpha}, \tag{A12}$$

where v_s is the 2D Fourier transform of the screened pseudopotential,

$$v_s(\vec{q},z) \equiv F_{2D}\left[\int d\vec{r}\,' \epsilon^{-1}(\vec{r},\vec{r}\,') \cdot v(\vec{r})\right]. \quad \text{(A13)}$$

In Appendix B we give the analytic form of Eq. (A13) when considering the Ashcroft pseudopotential and the Thomas-Fermi dielectric function.

2. Eliashberg function and lifetime broadening

An electronic state denoted (k_i,i) (momentum and and band index) can decay into another state (k_f,f) by emitting and absorbing phonons. We can write down the rate equation for the state occupancy applying first-order time-dependent perturbation theory.

We thus write (similarly as in Ref. 34)

$$\frac{\partial f(\epsilon_{i,\vec{k}_i})}{\partial t} = -F_- + F_+, \quad \text{(A14)}$$

where F_- indicates $(k_i,i) \rightarrow (k_f,f)$ kind of processes by emission or absorption of phonons,

$$F_- = +2\pi \sum_{f,\vec{q},\nu} f(\epsilon_{i,\vec{k}_i})[1-f(\epsilon_{f,\vec{k}_i-\vec{q}})]|g_{\vec{q},\nu}|^2 \{[n(\omega_{\vec{q},\nu})+1] \times \delta(\epsilon_{\vec{k}_i} - \epsilon_{\vec{k}_i-\vec{q}} - \omega_{\vec{q},\nu}) n(\omega_{\vec{q},\nu}) \delta(\epsilon_{\vec{k}_i} - \epsilon_{\vec{k}_i-\vec{q}} + \omega_{\vec{q},\nu})\}, \quad \text{(A15)}$$

and where F_+ indicates $(k_f,f) \rightarrow (k_i,i)$ kind of scattering,

$$F_+ = +2\pi \sum_{f,\vec{q},\nu} f(\epsilon_{f,\vec{k}_i-\vec{q}})[1-f(\epsilon_{i,\vec{k}_i})]|g_{\vec{q},\nu}|^2 \times \{n(\omega_{\vec{q},\nu}) \delta(\epsilon_{\vec{k}_i} - \epsilon_{\vec{k}_i-\vec{q}} - \omega_{\vec{q},\nu}) + [n(\omega_{\vec{q},\nu})+1] \delta(\epsilon_{\vec{k}_i} - \epsilon_{\vec{k}_i-\vec{q}} + \omega_{\vec{q},\nu})\}. \quad \text{(A16)}$$

$\vec{q}$ and ν refer to the phonon mode and polarization, and $(i,\vec{k}_i)$ and $(f,\vec{k}_f) \equiv (f,\vec{k}_i-\vec{q})$ pairs refer to the initial and final electronic band and momentum parallel to the surface.

If we consider the change of $f(\epsilon_{i,\vec{k}_i})$ in Eq. (A14) by an amount $\Delta f(\epsilon_{i,\vec{k}_i})$ from its equilibrium value and maintain $f(\epsilon_{f,\vec{k}_f})$ constant we can define the lifetime as follows:[34]

$$\frac{\partial f(\epsilon_{i,\vec{k}_i})}{\partial t} = -\frac{\Delta f(\epsilon_{i,\vec{k}_i})}{\tau(i,\vec{k}_i)}. \quad \text{(A17)}$$

From Eqs. (A14) and (A17) one then obtains for the lifetime broadening ($\Gamma = \tau^{-1}$)

$$\Gamma(\epsilon_{i,\vec{k}_i}) = 2\pi \int d^2\vec{q} \sum_{f,\vec{G}}^{\nu} |g^{i,f}_{\vec{q},\nu}|^2 O_+ \delta(\epsilon_{i,\vec{k}_i} - \epsilon_{f,\vec{k}_i-\vec{q}} - \omega_{\vec{q},\nu}) + O_- \delta(\epsilon_{i,\vec{k}_i} - \epsilon_{f,\vec{k}_i-\vec{q}} + \omega_{\vec{q},\nu})], \quad \text{(A18)}$$

where

$$O_+(\omega,\epsilon) \equiv n_B(\omega) + 1 - f(\epsilon),$$
$$O_-(\omega,\epsilon) \equiv n_B(\omega) + f(\epsilon). \quad \text{(A19)}$$

Equation (A18) is enough to calculate the lifetime broadening due to the e-p coupling at any temperature. However, to get a more physical picture we introduce the Eliashberg function and integrate over the energy exchange ω between the electrons and the phonons in the scattering events. According to the explicit form of the Eliashberg functions given in Eqs. (8) and (9), we thus obtain the final expression for the lifetime broadening,

$$\Gamma(\epsilon_{i,\vec{k}_i}) = 2\pi \left(\int_0^\infty \alpha^2 F^E_{i,\vec{k}_i}(\omega) O_+(\omega, \epsilon_{i,\vec{k}_i} - \omega) + \alpha^2 F^A_{i,\vec{k}_i}(\omega) O_-(\omega, \epsilon_{i,\vec{k}_i} + \omega) \right) d\omega. \quad \text{(A20)}$$

In a real calculation, the phonon energies appearing in Eqs. (8) and (9) can be neglected as they are in general small in comparison to the electron energies except for the case of near $\overline{\Gamma}$ point intraband scattering, that is when, $|k_i| \ll \sqrt{\omega_m}$. For interband scattering [$i \neq f$ in Eqs. (8) and (9)], one can safely make use of the elastic scattering approximation,

$$\delta(\epsilon_{i,\vec{k}_i} - \epsilon_{f,\vec{k}_i-\vec{q}} \pm \omega_{\vec{q},\nu}) \simeq \delta(\epsilon_{i,\vec{k}_i} - \epsilon_{f,\vec{k}_i-\vec{q}}), \quad \text{(A21)}$$

nevertheless, we calculate the emission and absorption Eliashberg functions as in Eqs. (8) and (9) for the intraband scattering.

APPENDIX B: 2D FOURIER TRANSFORMED THOMAS-FERMI SCREENED ASHCROFT PSEUDOPOTENTIAL

In this section we give some details for the pseudopotential gradient and its Fourier transform. We have used the Ashcroft empty core pseudopotential[38] defined as

$$v(r) = -Z_c \cdot \frac{\theta(r-R_c)}{r} = -Z_c \cdot \frac{\theta(\sqrt{x^2+z^2}-R_c)}{\sqrt{x^2+z^2}}, \quad \text{(B1)}$$

where $\vec{r} \equiv (\vec{x},z)$, $\theta(r)$ is the Heaviside function, Z_c is the valence of the element, and R_c is the ''core radius'' parameter fitted to experiment. The 3D Fourier transform of the Ashcroft pseudopotential is

$$v(q) = -\frac{4\pi Z_c}{q^2} \cos[qR_c]. \quad \text{(B2)}$$

The 3D Fourier transform of the screened pseudopotential with the Thomas-Fermi screening is

$$v_s(q) = \epsilon^{-1}(q) \cdot v_A(q) = -\frac{4\pi Z_c}{q^2+q_{TF}^2} \cdot \cos[qR_c]. \quad \text{(B3)}$$

We then perform the back Fourier transform in the z direction, retaining the parallel transformation, required in the presented formulation.

$$v_{s,A}(q,z) = -\frac{2\pi Z_c}{\sqrt{q^2+q_{TF}^2}} e^{-\sqrt{q^2+q_{TF}^2}|z|} \cdot \cosh[q_{TF}R_c] + 2\pi Z_c \theta(R_c-|z|) \int_0^{\sqrt{R_c^2-z^2}} \frac{J_0(qx)x}{\sqrt{x^2+z^2}} \times e^{q_{TF}(R_c-\sqrt{x^2+z^2})} dx. \quad \text{(B4)}$$

In the range of momentum transfers considered in this work [$|q_\parallel| \sim 1$ (a.u.)], a good approximation to this last expression is

$$v_{s,A}(q,z) \approx -\frac{2\pi Z_c}{\sqrt{q^2+q_{TF}^2}} e^{-\sqrt{q^2+q_{TF}^2}|z|} \cdot \cosh[q_{TF}R_c] + 2\pi Z_c \theta(|z|-R_c) \frac{\sinh[(R_c-|z|)q_{TF}]}{q_{TF}}, \quad \text{(B5)}$$

where $J_0(qx) \approx 1$ has been used.

[1] R. Matzdorf, Surf. Sci. Rep. **30**, 153 (1998).
[2] M. Bonn, S. Funk, Ch. Hess, D. N. Denzler, C. Stampfl, M. Scheffler, M. Wolf, and G. Ertl, Science **285**, 1042 (1999).
[3] L. Bürgi, O. Jeandupeux, H. Brune, and K. Kern, Phys. Rev. Lett. **82**, 4516 (1999).
[4] M. Bauer, S. Pawlik, and M. Aeschlimann, Phys. Rev. B **60**, 5016 (1999).
[5] H. Petek, M. J. Weida, H. Nagano, and S. Ogawa, Science **451**, 22 (2000).
[6] P. M. Echenique, J. M. Pitarke, E. V. Chulkov, and A. Rubio, Chem. Phys. **251**, 1 (2000).
[7] A. G. Borisov, A. K. Kazansky, and J. P. Gauyacq, Phys. Rev. Lett. **80**, 1996 (1998).
[8] A. Fukui, H. Kasai, and A. Okiji, J. Phys. Soc. Jpn. **70**, 29 (2001).
[9] E. V. Chulkov, V. M. Silkin, and M. Machado, Surf. Sci. **482-485**, 693 (2001).
[10] A. Fukui, H. Kasai, and A. Okiji, Surf. Sci. **493**, 671 (2001).
[11] H. Nienhaus, Surf. Sci. Rep. **45**, 1 (2002).
[12] P. M. Echenique and J. B. Pendry, J. Phys. C **11**, 2065 (1978).
[13] P. M. Echenique and J. B. Pendry, Prog. Surf. Sci. **32**, 111 (1990).
[14] J. Kliewer, R. Berndt, E. V. Chulkov, V. M. Silkin, P. M. Echenique, and S. Crampin, Science **288**, 1399 (2000).
[15] H. Hövel, B. Grimm, and B. Reihl, Surf. Sci. **477**, 43 (2001).
[16] V. Yu. Yurov, A. Bendownan, B. Kierren, Y. Fagot Revurat, F. Bertran, and D. Malterre, Phys. Low-Dimens. Semicond. Struct. **11/12**, 155 (2001).
[17] K. F. Braun and K. H. Rieder, Phys. Rev. Lett. **88**, 096801 (2002).
[18] K. Morgenstern, K. F. Braun, and K. H. Rieder, Phys. Rev. Lett. **89**, 226801 (2002).
[19] A. Bauer, A. Mühlig, D. Wegner, and G. Kaindl, Phys. Rev. B **65**, 075421 (2002).
[20] L. Vitali, P. Wahl, M. A. Schneider, K. Kern, V. M. Silkin, E. V. Chulkov, and P. M. Echenique, Surf. Sci. **523**, L47 (2003).
[21] B. A. McDougall, T. Balasubramanian, and E. Jensen, Phys. Rev. B **51**, 13 891 (1995).
[22] T. Valla, A. V. Fedorov, P. D. Johnson, and S. L. Hulbert, Phys. Rev. Lett. **83**, 2085 (1999).
[23] P. Straube, F. Pforte, T. Michalke, K. Berge, A. Gerlach, and A. Goldmann, Phys. Rev. B **61**, 14 072 (2000).
[24] F. Reinert, G. Nicolay, S. Schmidt, D. Ehm, and S. Hüfner, Phys. Rev. B **63**, 115415 (2001).
[25] T. Balasubramanian, L. I. Johansson, P. A. Glans, C. Virojanadara, V. M. Silkin, E. V. Chulkov, and P. M. Echenique, Phys. Rev. B **64**, 205401 (2001).
[26] V. M. Silkin, T. Balasubramanian, E. V. Chulkov, A. Rubio, and P. M. Echenique, Phys. Rev. B **64**, 085334 (2001).
[27] S. J. Tang, Ismail, P. T. Sprunger, and E. W. Plummer, Phys. Rev. B **65**, 235428 (2002).
[28] M. Hengsberger, D. Purdie, P. Segovia, M. Garnier, and Y. Baer, Phys. Rev. Lett. **83**, 592 (1999); M. Hengsberger, R. Fresard, D. Purdie, P. Segovia, and Y. Baer, Phys. Rev. B **60**, 10 796 (1999).
[29] E. Knoesel, A. Hotzel, and M. Wolf, J. Electron Spectrosc. Relat. Phenom. **88-91**, 577 (1998).
[30] A. Schäfer, I. L. Shumay, M. Wiets, M. Weinelt, Th. Fauster, E. V. Chulkov, V. M. Silkin, and P. M. Echenique, Phys. Rev. B **61**, 13 159 (2000).
[31] A. Eiguren, B. Hellsing, F. Reinert, G. Nicolay, E. V. Chulkov, V. M. Silkin, S. Hüfner, and P. M. Echenique, Phys. Rev. Lett. **88**, 066805 (2002).
[32] J. M. Ziman, *Electron and Phonons* (Clarendon, Oxford, 1960).
[33] *Electron-Electron and Electron-Phonon Interactions on the One-Electron States of Solids*, edited by L. Hedin and S. Lundqvist, Solid State Phys. **23**, 1 (1969).
[34] G. Grimvall, in *The Electron-Phonon Interaction in Metals*, *Selected Topics in Solid State Physics*, edited by E. Wohlfarth (North-Holland, New York, 1981).
[35] E. G. Maksimov, D. Yu Savrasov, and S. Yu Savrasov, Sov. Phys. Usp. **40**, 337 (1997).
[36] T. K. Mitra, J. Phys. C **2**, 52 (1969).
[37] *Solid State Physics*, edited by D. Turnbull and F. Seitz (Academic New York, 1970), Vol. 24.
[38] N. W. Ashcroft, Phys. Lett. **23**, 48 (1966).
[39] S. Andersson, B. N. J. Persson, M. Persson, and N. D. Lang, Phys. Rev. Lett. **52**, 2073 (1984).
[40] M. Persson, J. A. Stroscio, and W. Ho, Phys. Scr. **36**, 548 (1987).
[41] B. Hellsing, A. Eiguren, and E. Chulkov, J. Phys.: Condens. Matter **14**, 5959 (2002).
[42] G. D. Mahan, in *Many-Particle Physics* (Plenum, New York, 1990).
[43] E. V. Chulkov, V. M. Silkin, and P. M. Echenique, Surf. Sci. **437**, 330 (1999); **391**, L1217 (1997).
[44] E. V. Chulkov, I. Sarría, V. M. Silkin, J. M. Pitarke, and P. M. Echenique, Phys. Rev. Lett. **80**, 4947 (1998).
[45] U. Harten, J. P. Toennies, and Ch. Wöll, Faraday Discuss. Chem. Soc. **80**, 137 (1985).
[46] J. E. Black and F. C. Shanes, Surf. Sci. **133**, 199 (1983).
[47] S. Trullinger, J. Math. Phys. **17**, 1884 (1976).
[48] *The Modern Physics of Phonons: Transport, Surfaces and Simu-*

lations, *Dynamical Properties of Solids*, edited by G. K. Horton and A. A. Maradudin (North-Holland, Amsterdam, 1990), Vol. 6.
[49] R. E. Allen, G. P. Alldredge, and F. W. Wette, Phys. Rev. B **4**, 1648 (1971).
[50] T. S. Rahman and D. L. Mills, Phys. Rev. B **21**, 1432 (1980).
[51] S. Y. Savrasov and D. Y. Savrasov, Phys. Rev. B **54**, 16 487 (1996).
[52] R. Keyling, W. Schöne, and W. Ekardt, Chem. Phys. Lett. **354**, 376 (2002).
[53] H. J. Levinson, F. Greuter, and E. W. Plummer, Phys. Rev. B **27**, 727 (1983).
[54] S. D. Kevan, N. G. Stoffel, and N. V. Smith, Phys. Rev. B **31**, 1788 (1985).
[55] S. D. Kevan, Phys. Rev. Lett. **50**, 526 (1983).